Research Article | Vol. 31, No. 15 / 17 Jul 2023 / Optics Express 24404
Optics EXPRESS

# Design of high-efficiency and large-angle homo-metagratings for light source integration

WEI-CHENG TSAI,[1] YU-HENG HONG,[2,3] HAO-CHUNG KUO,[1,2,4] AND YAO-WEI HUANG[1,*]

[1]Department of Photonics, College of Electrical and Computer Engineering, National Yang Ming Chiao Tung University, Hsinchu 30010, Taiwan
[2]Semiconductor Research Center, Hon Hai Research Institute, Taipei 11492, Taiwan
[3]enoch.yh.hong@foxconn.com
[4]hckuo0206@nycu.edu.tw
[*]ywh@nycu.edu.tw

**Abstract:** Meta-optics integrated with light sources has gained significant attention. However, most focused on the efficiency of metasurfaces themselves, rather than the efficiency of integration. To design highly efficient beam deflection, we develop a scheme of homo-metagrating, involving the same material for meta-atoms, substrate, and top layer of the laser, to achieve near-unity power from light-emitting to metasurfaces. We utilize three degrees of freedom: overall add-on phase, parameters of meta-atoms in a period, and lattice arrangement. The overall efficiency of homo-metagratings is higher than that of hetero-metagratings. We believe our approach is capable of being implemented in various ultracompact optic systems.



## 1. Introduction

Light manipulated by metasurfaces has made waves in all-pervasive optical applications [1–5]. Metasurface thereby paves the ability to replace conventional optical components [6–9]. Among these demonstrations, efficiency is always a crucial issue as one of the most important performance metric that characterizes the performance of a device [10,11]. Nevertheless, most of these demonstrations focused on the efficiency of metasurfaces themselves, rather than the efficiency of integration in optic systems. Metasurfaces relate efficiency typically categorized into two main ways [12]: the absolute efficiency [13,14] and the relative efficiency [15,16]. However, both methods do not consider the issue of reflection loss happening at the source-air boundary and the air-substrate boundary. Thus, we propose an overall perspective with the estimation method, revamping the impedance mismatching and unifying the standard of efficiency. To standardize such estimation methods for efficiency, metagratings as one of the most basic light manipulations are employed. We perform this method in both homo-metagratings [17,18] and hetero-metagratings [13,16,19,20], where homo-/hetero- is referred to usage of same/different material(s) for building blocks and substrate in this article.

As shown in Fig. 1(a) when the light passes through the substrate, reflection loss results in a drop of absolute efficiency. To avoid refractive index matching problem, the integration of homo-metasurfaces with vertical cavity surface emitting laser (VCSEL) have been investigated [18,21]. By utilizing a homo-metagrating, a relative efficiency of 50% (absolute efficiency of approximately 34%) was achieved at a deflection angle of ~60° [18]. However, further optimization for the deflection efficiency of metasurfaces themselves has not yet been conducted.

In this paper, we numerically demonstrate high-efficiency homo-metagratings based on a simple forward design (rather than the inverse design method). We propose an optimization method and unify the standard of efficiency evaluation. Considering the issue of impedance matching, we propose the overall efficiency that involves the integration in optic systems. We introduce 3 degrees of freedom that provides room for optimization. Our simulation results show

#496042 https://doi.org/10.1364/OE.496042
Journal © 2023 Received 19 May 2023; revised 28 Jun 2023; accepted 1 Jul 2023; published 10 Jul 2023

Optics EXPRESS

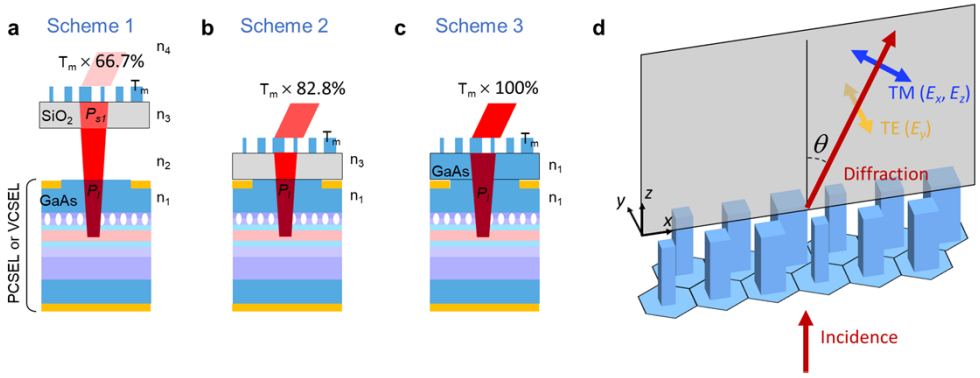


**Fig. 1.** Overview of metagrating design using our design. (a) When the light is deflected, the refractive index of the light is mismatched from the light source to the air. (b) Although the refractive index matching problem between the light source and the air is solved. The refractive index matching problem between the refractive index of silica and the material of the light source. (c) We designed metasurfaces with a refractive index similar to that of the light source. The refractive index of the light was matched from the light source to the metasurface. (d) When the incident light passes through the metasurfaces, the light has the TE TM mode beam in space because of the metasurfaces.

that a homo-metagrating can achieve a diffraction efficiency of 58% at the diffraction angle of 60°, which is approximately 1.7 times larger than that of homo-metagratings in the literature [18]. Such a comprehensive perspective is demonstrated, paving a promising path for future integration of optical systems, such as 3D sensing [22,23] and LiDAR [24].

## 2. Definition of overall efficiency

Many studies on efficiency of metasurfaces are focused on metasurfaces themselves, including building blocks and substrate. Therefore, a scheme of a higher index of nanostructures with a lower index of substrates (e.g., hetero-metagrating) was extensively considered. However, in the case of compact integration of metasurfaces and the light source, an overall efficiency considering light power from the source to the ideal order of beam deflection in the free space was necessary. Therefore, we compared the overall efficiency ($E_{overall}$) of three schemes. If we just simply integrated a high-efficiency metasurface (usually with a glass substate in the visible or near-infrared range) with a laser source separated with an air gap, as shown in Fig.1a, the overall efficiency is denoted as

$$E_{overall,1} = \frac{P_l \times T_{12} \times T_{23} \times T_m}{P_l} = T_{12} \times T_{23} \times T_m, \tag{1}$$

where $P_l$ represents the power of the laser light source. And $T_{ij}$ is the transmittance of light from one material (refractive index $n_i$) to another (refractive index $n_j$), that is

$$T_{ij} = \frac{4n_i n_j}{(n_i + n_j)^2}. \tag{2}$$

Here, $T_m$ represents the diffraction efficiency of metagratings (most in simulation), considering the light power from the substrate ($n_3$) through meta-atoms to the ideal order of beam deflection in the free space ($n_4$). If there are no meta-atoms on the substrate, $T_m$ becomes $T_{34}$. We assume a light beam with a wavelength of 940 nm illuminated from a VCSEL or a photonic crystal surface emitting laser (PCSEL) ($n_{GaAs} = 3.506$) to air; thus, the transmittance of the light is $T_{12} = 69.1\%$.

Optics EXPRESS

There is another transmittance from the air to the glass substate ($n_{glass} = 1.4512$), $T_{23} = 96.6\%$. Therefore, the overall efficiency became $E_{overall,1} = T_m \times 66.7\%$. Note that the absolute efficiency (most in experiment) of a metasurface is usually derived as $T_{23} \times T_m$ and the relative efficiency (most in experiment) of a metasurface is usually derived as $(T_{23} \times T_m) / (T_{23} \times T_{34}) = T_m / T_{34}$.

If the hetero-metagrating and the light source are connected, as shown in Fig. 1(b), there is only one material boundary (GaAs and the glass substate). Therefore, the overall efficiency in Scheme 2 is denoted as follow:

$$E_{overall,2} = \frac{P_l \times T_{13} \times T_m}{P_l} = T_{13} \times T_m. \tag{3}$$

The overall efficiency was expected to be improved as compared to that of Scheme 1. The light is incident from the light source to the glass substrate, the transmittance of the light is $T_{13} = 82.8\%$, and the overall efficiency increases to $E_{overall,2} = T_m \times 82.8\%$.

To further enhance the overall efficiency, we replace the substrate with GaAs, as shown in Fig. 1(c). The overall efficiency in Scheme 3 is denoted as

$$E_{overall,3} = \frac{P_l \times T_m}{P_l} = T_m. \tag{4}$$

There is no boundary of materials with a different refractive index from light source to the substate. Therefore, the overall efficiency further increases to $E_{overall,3} = T_m \times 100\%$, which is considerably higher than that in Schemes 1 and 2.

Although the meta-atoms we selected are polarization insensitive, the deflected beam is indeed polarization sensitive. If we consider the principle of reversibility, deflection beam follows the same path but reverses its direction of travel. The reversed direction of travel is tilted with respect to the meta-atoms' axes, resulting in not strictly polarization independent even if meta-atoms are polarization insensitive [25]. For instance, in Fig. 1(d), a beam illuminated to $z$-direction is deflected to the $x$-direction with diffraction angle $\theta$, the $x$–$z$ plane is defined as a diffraction plane. Therefore, the TE and TM modes are defined as the polarization states of light where the electric fields are perpendicular and parallel to the diffraction plane.

## 3. Design of meta-atoms

To determine meta-atoms for our metagrating, we use the RETICOLO package to calculate the transmittance and phase versus the different geometry parameters of nanopillars [26]. The material of the nanopillars and substrate that we simulated are GaAs (Scheme 3, Fig. 1(c)). Figure 2(a) shows the calculated transmission and phase coverage of square GaAs nanopillars as a function of width operating at the wavelength of 940 nm, which matches the working wavelength of PCSELs and VCSELs. The nanopillars are assembled in a subwavelength hexagonal lattice (Fig. 2(a)), fixing the distance between the adjacent nanopillars at 310 nm. The inset represents a single nanopillar of the array with width ranging from 80 nm to the lattice constant ($U$) of meta-atoms minus 100 nm, considering limitation in fabrication process of GaAs homo-metasurfaces (composed of circular or square nanopillars) [27]. We selected nanopillars that have phase coverage more than $2\pi$ while maintaining high efficiency, shown Fig. 2(a). The transmittance is not identity, which changed with the width of the nanopillar. A larger phase coverage provides us more degree of freedom (DOF) in the nanopillar sampling. The two factors caused differences in the diffraction efficiency, especially when select a few pillars for forming a metagrating.

Optics EXPRESS

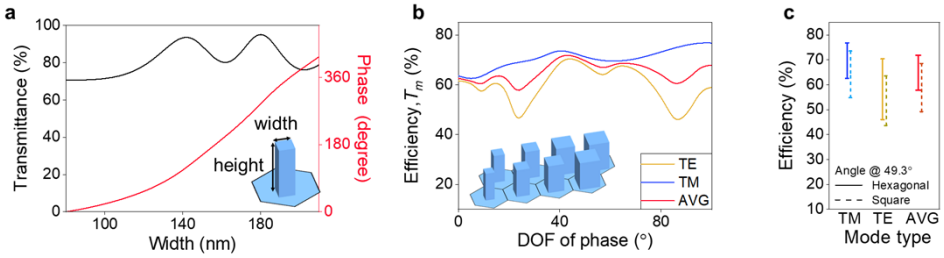


**Fig. 2.** (a) Calculated transmission and phase coverage of square GaAs nanopillars as a function of the width operating at the wavelength of 940 nm. The inset represents a nanopillar in hexagonal arrangement. (b) Simulated diffraction efficiency (at TM mode, TE mode, and their average) at deflection angle of 49.3° versus different DOF of phase. (c) Comparison of range of diffraction efficiency at TM mode, TE mode, and their average in hexagonal and square arrangement.

## 4. Design of metagrating based on DOF of phase

These nanopillars are not limited to a square shape. We also calculated the transmittance and the phase of circular nanopillars. Moreover, nanopillars with different periodicities as well as lattice arrangements were considered in the calculation. First, we designed a grating in the hexagonal lattice by using our designed meta-atoms that geometric parameters mentioned in session 3. For instance, the number of meta-atoms in a supercell in $x$-direction is $N$, the lattice constant of the meta-atoms is represented by $U$, and the grating period was therefore represented by $\Lambda = N \times U$. The deflection angle ($\theta$) is derived as

$$\theta = \sin^{-1}\left(\frac{\lambda}{\Lambda}\right) = \sin^{-1}\left(\frac{\lambda}{NU}\right). \tag{5}$$

We therefore control the different diffraction angles by using different numbers of unit cells ($N$) and lattice constant ($U$). The ideal phase distribution of the metagrating is defined as

$$\Phi_{deflector}(x) = \frac{2\pi}{\lambda} x \sin\theta + \delta, \tag{6}$$

where $\delta$ is a constant respected to the position and can be any value, denoting the DOF of the overall add-on phase (hereinafter referred to as DOF of phase). Different nanopillars had different transmittance values. Therefore, selecting different set of nanopillars by manipulating different $\delta$ leads to higher efficiency.

To compare the diffraction efficiency of the grating versus the DOF of the phase, we calculate the diffraction efficiency in TM and TE modes at a fixed deflection angle of 49.3° ($U = 310$ nm and $N = 4$). The results are shown in Fig. 2(b). We observed that the diffraction efficiency varies by changing the DOF of the phase. This result confirmed that the diffraction efficiency varied during the selection of a few pillars for forming a metagrating. Moreover, the maximum diffraction efficiency of the TM mode was higher than that of the TE mode.

Different lattice arrangements affect the efficiency too. We also calculated the diffraction efficiency of the grating in the square lattice arrangement (same periodicity and diffraction angle). The results are presented in Fig. 2(c). The efficiency still varies by changing the DOF of the phase. We observed that the overall efficiency of the square lattice was lower than that of the hexagonal arrangement in this case. We will compare more cases in Section 5.

To see how different shapes of nanopillars affects the efficiency, we also calculate the diffraction efficiency of the square and circular nanopillars in the TM (blue line) and TE (amber line) modes, as shown in Figs. 3(a) and 3(b), respectively. Each efficiency range at each diffraction angle

Optics EXPRESS

indicates results from different DOFs of the phase. The deflection angle is related to $N$ and $U$, where $N = 3$–$9$ and $U = 300$–$390$ nm is considered. We observe that the efficiency of the grating is similar with different patterns (square nanopillars and circular pillars). As shown in Figs. 3(a) and 3(b), the maximum diffraction efficiency of the TM mode is generally higher than that of the TE mode. This meant that we could obtain a higher efficiency of deflection beams by controlling the orientation of the meta-grating parallel to the linearly polarized beam from the mode controllable VCSEL or PCSEL.

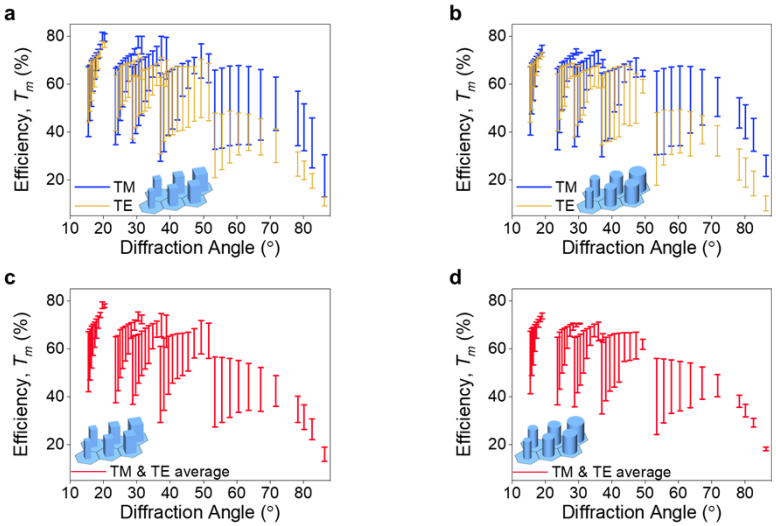


**Fig. 3.** Simulated metagrating efficiency analysis. Simulated diffraction efficiency at TM and TE mode of metagrating of (a) square nanopillars and (b) circle nanopillars. (c) Average efficiency of metagrating of square nanopillars and (d) circle nanopillars.

Considering an unpolarized light incidence, we average diffraction efficiency in TM mode and TE mode in Figs. 3(c) (square nanopillars) and 3d (circular nanopillars). If the incident light from laser source is a plane wave, the overall deflection efficiency ($E_{overall,3}$) is up to 58.9% at a diffraction angle of 60° (in both Figs. 3(c) and 3(d)). This value is about 85% in relative efficiency, which is 1.7 times larger than literature [18]. This result reveals that the metasurfaces designed by the simple forward optimization based on the DOF of the phase could realize a highly efficient metasurface even at a large diffraction angle. Moreover, this design could be used to directly manufacture metasurfaces on the light source to achieve the integration of the light source and the diffractive component.

## 5. Design of metagrating based on more DOFs

There are more degrees of freedom utilized to increase the deflection efficiency rather than the DOF of phase. For example, a diffraction angle is determined by using the grating period $\Lambda$, which is obtained with different sets of $N$ and $U$. We calculate the peak average efficiency for $N = 5$ and $N = 6$, and the efficiency versus deflection angle is shown in Fig. 4(a). A deflection angle of ~28.8°, for instance, can be realized by setting ($N$, $U$) = (5, 310 nm) or (6, 370 nm). However, the set of (5, 310 nm) results in higher efficiency. Therefore, the deflection angle ranges from 28.8° to 30.5° (marked with light red background) indicated that the DOF in the selection of ($N$, $U$) played an important role in determining the efficiency as well as the DOF of phase. In contrast, both the profiles ($N = 5$ and $N = 6$) has peak efficiency at $U = 310$ nm, which could be attributed to the higher transmission of nanopillars with a specific lattice constant of meta-atoms.

Optics EXPRESS

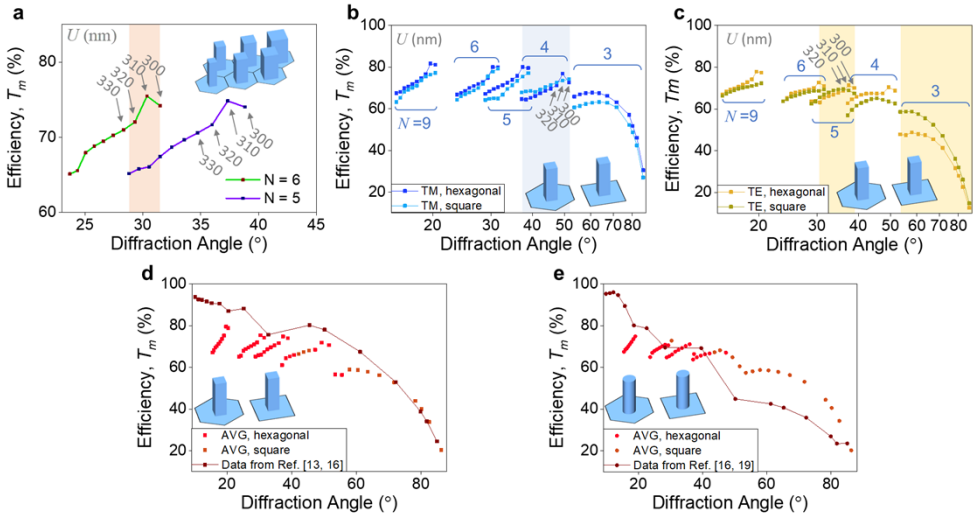


**Fig. 4.** Comparison of lattice and efficiency. (a) In the similar diffraction angle range, the DOF can be used to obtain better diffraction efficiency. We simulated the arrangement of hexagonal and square lattices as a degree of freedom to select better (b) TM and (c) TE diffraction efficiency. Comparison of the average efficiency of hetero-metagratings from Ref. [16] with our design of homo-metagratings, where the homo-metagratings consist of (d) square nanopillars and (e) circle nanopillars arranged in both hexagonal and square lattices.

Arrangement of nanopillars provides another DOF in design. We also simulate a homo-metagrating made of square nanopillars arranged in a square lattice and compare the highest efficiency in TM mode with that in a hexagonal one, shown in Fig. 4(b). Overall, hexagonal lattice arrangement performs efficiency higher than that of square lattice in most of cases of $N$. In contrast, square lattice arrangement is higher at $N = 4$ (marked with light blue background), except ($N$, $U$) = (4, 310 nm), which detail results shown in Figs. 2(b) and 2(c). On the other hand, we compare the efficiency in TE mode and results are shown in Fig. 4(c). Hexagonal lattice arrangement has higher efficiency as well except $N = 3$ and 5 (marked with light amber background). This indicated that the arrangement of the lattice serves as a DOF for higher diffraction efficiency in design.

Next, we compare the average efficiency of our homo-metagrating with that of the hetero-metagrating from Ref [13,16,19]., as shown in in Figs. 4(d) and 4(e). Considering an integration of homo-metagrating and light source, the overall efficiency for homo-metagrating is $E_{overall,3} = T_m$. In contrast, that is $E_{overall,1} = T_{23} \times T_m$ for integration of hetero-metagrating and light source. We assume $T_{12} = 1$ here, but light extraction efficiency of lasers is not unity and changes with different lasers. We found that the overall efficiency of our homo-metagrating (square nanopillars) achieved results similar to those reported in Ref. [16] (Fig. 4(d)). On the other hand, our homo-metagrating (circular nanopillars) performs significant high overall efficiency at diffraction angles larger than 40° compared to [16] (Fig. 4(e)). If we consider the refractive index difference ($n_1 \neq n_2$, $T_{12} < 1$) at laser-air boundary, the overall efficiency of hetero-metagratings is even lower, indicating the significant overall efficiency improvement with homo-metagratings in our design.

## 6. Conclusion

In this study, we demonstrated high-efficiency homo-metagratings based on a simple forward optimization design through simulations. We forward optimize homo-metagratings by utilizing

Optics EXPRESS

the DOF of phase ($\delta$), number of unit cells ($N$), lattice constant ($U$), and lattice arrangement. The simulated diffraction efficiency gets up to 67.7% and 58.6% for the TM mode and average at a deflection angle of ~60° (Fig. 4(b)) [18]. It means that usage of a polarization characteristics of laser (e.g., PCSEL) in the integration can further increase the diffraction efficiency [28]. The homo-metagratings can solve the problem of reduced diffraction efficiency caused by packaged light sources passing through the substrate and the metasurfaces by allowing for the direct fabrication of a metasurface onto the unpackaged GaAs materials, such as PCSEL or VCSEL [29,30]. The overall efficiency of homo-metagratings can be even increased by using inverse design that provides more degrees of freedom in geometric shapes not intuitively driven by humans [16,31,32]. There is a high potential for the integration of the metasurfaces into PCSEL or VCSEL for research applications such as LiDAR, depth sensing, and optical communication.

**Funding.** National Science and Technology Council (110-2112-M-A49-034-MY3, 110-2622-8-A49-008-SB, 111-2622-8-A49-021-SB).

**Acknowledgments.** The authors acknowledge support from the National Science and Technology Council in Taiwan and the Ministry of Education in Taiwan under the Yushan Young Scholar Program. The authors also acknowledge the Semiconductor Research Center, Hon Hai Research Institute for their technical support.

**Disclosures.** The authors have no conflicts of interest to declare.

**Data availability.** Data underlying the results presented in this paper are not publicly available at this time but may be obtained from the authors upon reasonable request.

## References

1. Y.-H. Hong, W.-C. Hsu, W.-C. Tsai, Y.-W. Huang, S.-C. Chen, and H.-C. Kuo, "Ultracompact nanophotonics: light emission and manipulation with metasurfaces," Nanoscale Res. Lett. **17**(1), 41 (2022).
2. H.-H. Hsiao, C. H. Chu, and D. P. Tsai, "Fundamentals and applications of metasurfaces," Small Methods **1**(4), 1600064 (2017).
3. L. Zhang, S. Mei, K. Huang, and C.-W. Qiu, "Advances in full Control of electromagnetic waves with metasurfaces," Adv. Opt. Mater. **4**(6), 818–833 (2016).
4. S. M. Kamali, E. Arbabi, A. Arbabi, and A. Faraon, "A review of dielectric optical metasurfaces for wavefront control," Nanophotonics **7**(6), 1041–1068 (2018).
5. N. Yu and F. Capasso, "Flat optics with designer metasurfaces," Nat. Mater. **13**(2), 139–150 (2014).
6. P. C. Wu, W.-Y. Tsai, W. T. Chen, Y.-W. Huang, T.-Y. Chen, J.-W. Chen, C. Y. Liao, C. H. Chu, G. Sun, and D. P. Tsai, "Versatile polarization generation with an aluminum plasmonic metasurface," Nano Lett. **17**(1), 445–452 (2017).
7. Y.-W. Huang, W. T. Chen, W.-Y. Tsai, P. C. Wu, C.-M. Wang, G. Sun, and D. P. Tsai, "Aluminum plasmonic multicolor meta-hologram," Nano Lett. **15**(5), 3122–3127 (2015).
8. C.-F. Chen, C.-T. Ku, Y.-H. Tai, P.-K. Wei, H.-N. Lin, and C.-B. Huang, "Creating optical near-field orbital angular momentum in a gold metasurface," Nano Lett. **15**(4), 2746–2750 (2015).
9. Z. Li, P. Lin, Y.-W. Huang, J.-S. Park, W. T. Chen, Z. Shi, C.-W. Qiu, J.-X. Cheng, and F. Capasso, "Meta-optics achieves RGB-achromatic focusing for virtual reality," Sci. Adv. **7**(5), eabe4458 (2021).
10. G. Zheng, H. Mühlenbernd, M. Kenney, G. Li, T. Zentgraf, and S. Zhang, "Metasurface holograms reaching 80% efficiency," Nat. Nanotechnol. **10**(4), 308–312 (2015).
11. M. Mansouree, A. McClung, S. Samudrala, and A. Arbabi, "Large-scale parametrized metasurface design using adjoint optimization," ACS Photonics **8**(2), 455–463 (2021).
12. P. Lalanne and P. Chavel, "Metalenses at visible wavelengths: past, present, perspectives," Laser Photonics Rev. **11**(3), 1600295 (2017).
13. P. Lalanne, S. Astilean, P. Chavel, E. Cambril, and H. Launois, "Design and fabrication of blazed binary diffractive elements with sampling periods smaller than the structural cutoff," J. Opt. Soc. Am. A **16**(5), 1143–1156 (1999).
14. Y. Hu, L. Li, Y. Wang, M. Meng, L. Jin, X. Luo, Y. Chen, X. Li, S. Xiao, H. Wang, Y. Luo, C.-W. Qiu, and H. Duan, "Trichromatic and tripolarization-channel holography with noninterleaved dielectric metasurface," Nano Lett. **20**(2), 994–1002 (2020).
15. M. Khorasaninejad, W. T. Chen, R. C. Devlin, J. Oh, A. Y. Zhu, and F. Capasso, "Metalenses at visible wavelengths: diffraction-limited focusing and subwavelength resolution imaging," Science **352**(6290), 1190–1194 (2016).
16. D. Sell, J. Yang, S. Doshay, R. Yang, and J. A. Fan, "Large-angle, multifunctional metagratings based on freeform multimode geometries," Nano Lett. **17**(6), 3752–3757 (2017).
17. Y.-Y. Xie, P.-N. Ni, Q.-H. Wang, Q. Kan, G. Briere, P.-P. Chen, Z.-Z. Zhao, A. Delga, H.-R. Ren, H.-D. Chen, C. Xu, and P. Genevet, "Metasurface-integrated vertical cavity surface-emitting lasers for programmable directional lasing emissions," Nat. Nanotechnol. **15**(2), 125–130 (2020).
18. Q.-H. Wang, P.-N. Ni, Y.-Y. Xie, Q. Kan, P.-P. Chen, P. Fu, J. Deng, T.-L. Jin, H.-D. Chen, H. W. H. Lee, C. Xu, and P. Genevet, "On-chip generation of structured light based on metasurface optoelectronic integration," Laser Photonics Rev. **15**(3), 2000385 (2021).

Optics EXPRESS


19. A. Arbabi, Y. Horie, A. J. Ball, M. Bagheri, and A. Faraon, "Subwavelength-thick lenses with high numerical apertures and large efficiency based on high-contrast transmitarrays," Nat. Commun. **6**(1), 7069 (2015).
20. R. A. Aoni, M. Rahmani, L. Xu, K. Zangeneh Kamali, A. Komar, J. Yan, D. Neshev, and A. E. Miroshnichenko, "High-efficiency visible light manipulation using dielectric metasurfaces," Sci. Rep. **9**(1), 6510 (2019).
21. P.-N. Ni, P. Fu, P.-P. Chen, C. Xu, Y.-Y. Xie, and P. Genevet, "Spin-decoupling of vertical cavity surface-emitting lasers with complete phase modulation using on-chip integrated Jones matrix metasurfaces," Nat. Commun. **13**(1), 7795 (2022).
22. Z. Li, Q. Dai, M. Q. Mehmood, G. Hu, B. L. Yanchuk, J. Tao, C. Hao, I. Kim, H. Jeong, G. Zheng, S. Yu, A. Alù, J. Rho, and C.-W. Qiu, "Full-space cloud of random points with a scrambling metasurface," Light: Sci. Appl. **7**(1), 63 (2018).
23. G. Kim, Y. Kim, J. Yun, S.-W. Moon, S. Kim, J. Kim, J. Park, T. Badloe, I. Kim, and J. Rho, "Metasurface-driven full-space structured light for three-dimensional imaging," Nat. Commun. **13**(1), 5920 (2022).
24. I. Kim, R. J. Martins, J. Jang, T. Badloe, S. Khadir, H.-Y. Jung, H. Kim, J. Kim, P. Genevet, and J. Rho, "Nanophotonics for light detection and ranging technology," Nat. Nanotechnol. **16**(5), 508–524 (2021).
25. H. Pahlevaninezhad, M. Khorasaninejad, Y.-W. Huang, Z. Shi, L. P. Hariri, D. C. Adams, V. Ding, A. Zhu, C.-W. Qiu, F. Capasso, and M. J. Suter, "Nano-optic endoscope for high-resolution optical coherence tomography in vivo," Nat. Photonics **12**(9), 540–547 (2018).
26. J. P. Hugonin and P. Lalanne, "RETICOLO software for grating analysis," arXiv, arXiv:2101.00901 (2023).
27. W.-C. Hsu, C.-H. Chang, Y.-H. Hong, H.-C. Kuo, and Y.-W. Huang, "Compact structured light generation based on meta-hologram PCSEL integration," Discover Nano **18**(1), 87 (2023).
28. Y. Liang, C. Peng, K. Sakai, S. Iwahashi, and S. Noda, "Three-dimensional coupled-wave model for square-lattice photonic crystal lasers with transverse electric polarization: A general approach," Phys. Rev. B **84**(19), 195119 (2011).
29. D. Wen, J. Meng, J. J. Cadusch, and K. B. Crozier, "VCSELs with on-facet metasurfaces for polarization state generation and detection," Adv. Opt. Mater. **9**(9), 2001780 (2021).
30. L.-R. Chen, C.-J. Chang, K.-B. Hong, W.-C. Weng, B.-H. Chuang, Y.-W. Huang, and T.-C. Lu, "Static beam steering by applying metasurfaces on photonic-crystal surface-emitting Lasers," J. Lightwave Technol. **40**(21), 7136–7141 (2022).
31. R. Pestourie, C. Pérez-Arancibia, Z. Lin, W. Shin, F. Capasso, and S. G. Johnson, "Inverse design of large-area metasurfaces," Opt. Express **26**(26), 33732–33747 (2018).
32. C.-H. Lin, Y.-S. Chen, J.-T. Lin, H. C. Wu, H.-T. Kuo, C.-F. Lin, P. Chen, and P. C. Wu, "Automatic inverse design of high-performance beam-steering metasurfaces via genetic-type tree optimization," Nano Lett. **21**(12), 4981–4989 (2021).